

Article

The Effect of CaO on the CO and NO_x Emission Characteristics of Fast-Growing Grass Combustion

Yan Li, Qingchao Hong, Haili Liu * and Heyun Liu

School of Energy and Mechanical Engineering, Hunan University of Humanities, Science and Technology, Loudi 417000, China

* Correspondence: liuhaili@huhst.edu.cn

Abstract: Fast-growing grass is a biomass material with characteristics such as high temperature and drought resistance; rapid growth and development; and repeated germination and cutting. Therefore, it is a popular biomass fuel. It is required that the pollutants produced during the biomass combustion process are appropriately controlled. For this purpose, our study analyses the influence of combustion temperature and calcium oxide (CaO) on the nitrogen oxides (NO_x) and carbon monoxide (CO) emission characteristics of fast-growing grass combustion using the biomass combustion flue gas analysis and testing platform. The results of our analysis revealed that CaO additive can simultaneously reduce the peak and total NO_x emissions at 750 °C. Particularly, 5% CaO demonstrated a significant control effect on the NO_x emission from the fast-growing grass combustion process, with a peak and total emissions reduction of 47.05% and 56.81%, respectively. In addition, with an increase in temperature, the CO emission curve attains a second peak higher than the first peak, and the peak and total emissions show a decreasing trend.

Keywords: temperature; CaO; fast-growing grass; combustion; CO; NO_x



Citation: Li, Y.; Hong, Q.; Liu, H.; Liu, H. The Effect of CaO on the CO and NO_x Emission Characteristics of Fast-Growing Grass Combustion. *Processes* **2023**, *11*, 760. <https://doi.org/10.3390/pr11030760>

Academic Editors: Adam Smoliński and Vladimir S. Arutyunov

Received: 14 December 2022

Revised: 22 February 2023

Accepted: 2 March 2023

Published: 4 March 2023



Copyright: © 2023 by the authors. Licensee MDPI, Basel, Switzerland. This article is an open access article distributed under the terms and conditions of the Creative Commons Attribution (CC BY) license (<https://creativecommons.org/licenses/by/4.0/>).

1. Introduction

In recent years, especially with the rapid development of the world economy and advancement in technology, the demand for energy among humans has been on the increase. Moreover, the continuous consumption of fossil fuels poses a series of environmental problems [1]. According to the statistics of the International Energy Agency, global energy demand and emissions increased by 5% in 2021, compared with 2020 [2], to about the same level attained before the new corona pneumonia epidemic (around 3.3 billion tonnes). Thus, to deal with this energy crisis and environmental problems, it is necessary to adjust the energy structure actively and develop renewable energy vigorously. Interestingly, biomass energy is an ideal alternative energy source because of its wide distribution, rich raw materials, and low pollution [3–6]. Specifically, compared with other types of biomass, fast-growing grass is characterized by high temperature and drought resistance; rapid growth and development; and repeated germination and cutting [7–9], which can quickly capture and fix carbon and regulate the atmospheric greenhouse effect. As a biomass fuel, fast-growing grass has the disadvantages such as low calorific value, low bulk density, and being difficult to collect and transport. It can be used as a soil remediation crop in abandoned mining areas and a stable fuel for biomass power plants if planted on a large scale. In addition, it can grow to about 4–5 m in height and 50–60 mm in diameter, which is highly suitable for biomass feedstock. It can also be used as asphalt, wall materials, wood-plastic composites, etc. [10–12].

Furthermore, the methods to utilize biomass resources include gasification, pyrolysis, direct combustion, etc. [13]. Among them, direct combustion technology is the most widely used method at present. This is because steam heat generated via burning biomass can operate steam turbines and generate electricity, thus, converting biomass energy into

electrical energy [5]. However, the utilization of biomass energy is accompanied by the emissions of pollutants, such as nitrogen oxides, sulfur oxides, and particulate dust. Besides environmental pollution, these pollutants may also cause harm to the environment and, much more, human health. Specifically, nitrogen oxides (NO_x) not only cause acid rain and haze, but they also increase the content of $\text{PM}_{2.5}$ in the atmosphere [14] and, much more, reacts with hydrocarbons to produce photochemical smog [15,16]. Moreover, carbon monoxide (CO) is a colorless, odorless, and non-irritating toxic gas, which is almost insoluble in water. In addition, it does not easily react with other substances in the air and can remain in the atmosphere for 2–3 years. Therefore, it is harmful to human health in the case of severe local pollution. Although the environmental protection work in China has made some progress, this environmental situation is still grim.

Nevertheless, for NO_x emission control, many scholars have found that the appropriate utilization of additives can effectively reduce the NO_x emission produced by biomass fuels [8]. Many scholars [17–21] have studied the effect of additives on the wet denitrification reaction. Specifically, the direct use of the additives is favored by a variety of scholars due to ease of operation, convenience, low cost, and small space occupation. For example, Chen [22] achieved better NO_x emission reduction via mixed combustion with a 5% additive in microalgae. Particularly, the results of the analysis show that the reduction order of the NO_x emission peak is $\text{CuCl}_2 > \text{SiC} > \text{ZnCl}_2 > \text{MgO}$. In addition, Liu [23] found that Na_2CO_3 and K_2CO_3 additives have certain catalytic reduction and immobilization effects on NO_x release during litchi peel combustion. In addition, Burak [24] found that $\text{AlNH}_4(\text{SO}_4)_2$ and NH_4MgPO_4 additives can reduce the conversion rate of fuel-N to NO in the sunflower shell combustion process by 40%. Furthermore, Liu [25] studied the emission characteristics of NO_x and N_2O in the fluidized combustion process of rice straw and pine sawdust after adding limestone at 800 °C. It was found that introducing limestone into the circulating fluidized bed (CFB) reactor reduced the NO emission. In addition, it was observed that when the Ca/S molar ratio was 2:1, 5:1, and 10:1, the NO reduction rates were 11.8, 15.1, and 24.9%, respectively. In addition, a ceramic-supported platinum catalyst on a ceramic carrier (TiO_2 , MnO_2), such as $\text{Cu}(\text{NO}_3)_2 \cdot 3\text{H}_2\text{O}$, H_2PtCl_6 , and 99.5% pure urea solutions can reduce the emissions of polluting gases such as NO_x [26–28].

Furthermore, a series of research works have been conducted on calcium-based additives. For example, Meng et al. [29] used CaO and MgO or kaolin as additives for biomass particle combustion and discovered that the additive of MgO can reduce the content of K and Cl in ash. In addition, Lindstrom et al. [30] mixed CaO with grains rich in alkali elements, such as barley and oats, for combustion. The results demonstrated that lime contributes to the formation of high-temperature molten potassium calcium phosphate, which slows ash deposition. In addition, Tomáš et al. [31] studied the effect of catalytic additives, such as calcium oxide (CaO) and potassium permanganate (KMnO_4), on the emissions of wheat bran and beet pulp particles by using a low-power boiler. The results of their research revealed that the additive of 15% CaO and 5% KMnO_4 could minimize NO_x emission. Much more, Zhang et al. studied the migration characteristics of sulfur and nitrogen during the combustion process of sludge with CaO additive. The results showed that in addition to promoting the conversion of HCN to other nitrogen-contained gases, CaO can promote the formation of NO from HCN and NH_3 ; and, much more, facilitate the reduction reaction of NO to N_2 [32]. Further still, Liu [33] investigated the catalytic effect of a regulator (CaO) on nitrogen conversion during sewage sludge pyrolysis and discovered that CaO usage is a promising strategy to effectively reduce the production of NO_x precursors and, much more, increase the generation of pollution-free N_2 .

Regarding the reduction of CO emission, most authors have focused on controlling combustion temperature and air flow [34]; moreover, it is also possible to reduce CO emission by adding CaO. For example, Hayhurst et al. [35] in their work, were able to half the concentration of CO after introducing CaO. More so, Leckner et al. [36] found that a 165 MW CFB boiler emits a significantly lower concentration of CO when some CaO was present in the bed layer. However, they did not consider the effect of different amounts of

CaO on CO emission. Thus, there exists a gap in the study of the effect of additives on the NO_x and CO emission characteristics of fast-growing grass combustion.

To bridge this gap, using fast-growing grass as our biomass material, we investigate the NO_x and CO emission characteristics at different combustion temperatures (600, 700, 750, 800, and 850 °C) and of different mass fractions (3, 5, 10, and 15%) of CaO additives at 750 °C. The experiment is conducted using a self-built tube furnace to provide some data references for the emission control of NO_x and CO during the combustion process and a theoretical basis for its efficient and low-pollution combustion.

2. Materials and Methods

2.1. Materials

The experimental samples of fast-growing grass were taken from a planting base in Yangshi Town, Loudi, Hunan Province, China. Subsequently, they were rinsed and pretreated before the experiment. First, the samples were thermally dried at 106 °C in an electric drying oven for 12 h; afterward, the samples were broken using a disintegrator (model: dfy-300) and sieved with an 80-mesh screen to achieve particles with diameters less than 200 μm ; they were well labeled and placed in a dry ware for later use. Specifically, the additive applied was reagent grade (AR) CaO with a purity greater than 98.0%. During the experiment, two types of samples were put to the test: (1) pure fast-growing grass samples; (2) a combination of fast-growing grass samples and CaO additives, with mass fractions of 3, 5, 10, and 15%, respectively.

A muffle furnace (model: 5E-MF6100) was employed for industrial analysis. In addition, the volatile content was measured according to the ASTM E0870-82R98E01 standard; the ash content was measured according to the ASTM E1755-01 standard; the fixed carbon content was obtained by difference method. Furthermore, the elemental analysis was performed using an elemental analyzer (model: Vario EL cube); the calorimeter (model: WZR-1TCII) was used to measure the upper calorific value, and the results are shown in Figure 1. In Figure 1, it is shown that fast-growing grass had a lower ash content and higher volatile content and was prone to pyrolysis.

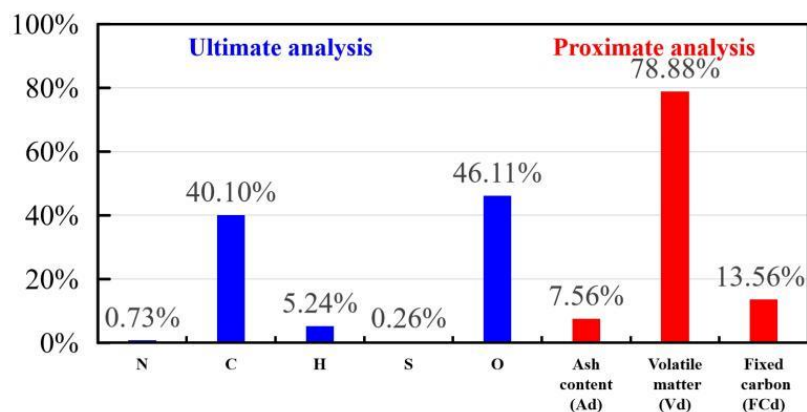


Figure 1. The ultimate and proximate analysis of fast-growing grass samples (% dry weight).

2.2. Apparatus and Methods

The schematic diagram of the experimental system is shown in Figure 2. Specifically, the combustion experiment was conducted using a quartz tube reactor in a tubular furnace (OTF-1200X) with a length of 600 mm and an inner diameter of 43 mm. Consequently, the NO_x and CO emissions were measured by the flue gas analyzer (Testo 350), and the data were monitored at the computer terminal.

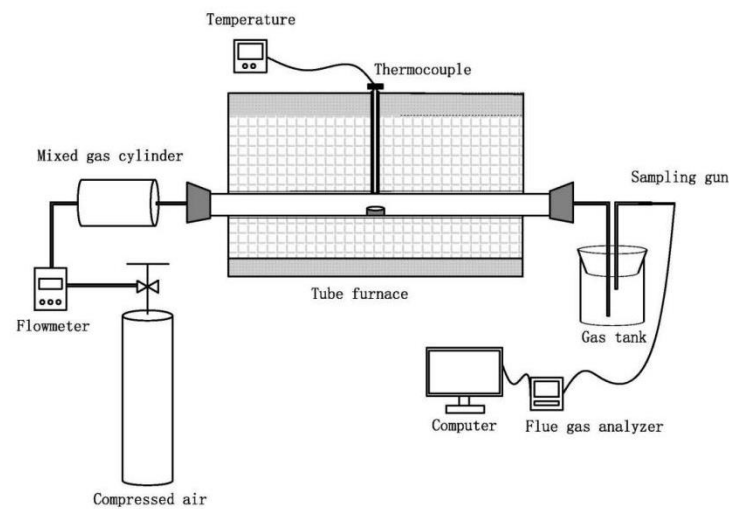


Figure 2. Schematic diagram of the experimental system.

The specific experimental steps are as follows: we set the experimental target temperature on the temperature control box of the tubular furnace; thereafter, using the flowmeter, we opened the air valve and control the flow of O₂ and N₂ to 0.2 and 0.8 L/min, respectively; after the temperature rose to the specified temperature, we weighed 0.2 g of the sample and corresponding proportion of CaO, laid them in the porcelain boat and stirred them for 100 times with a spoon; after this, we used the flue gas analyzer probe to measure the NO_x and CO emissions at the flue gas outlet, and then monitored the data in real-time; the combustion reaction was deemed to be finished when the CO and NO_x volume concentrations fell to 2 ppm. To reduce the error, each group conducted three experiments and took the average value.

2.3. Calculation Method

When the concentrations of CO and NO_x emission dropped to 2 ppm, the combustion reaction was regarded to be finished, according to the experimental method. The time spent was thus the burnout time, which is noted as τ . We may refer to Liu [37] and Xu [38] for the calculation formula. The calculation method of the CO parameters is consistent with that of the NO_x parameters.

(1) The average concentration C_{AC}

$$C_{AC} = \frac{\int_0^t C dt}{\tau} \quad (1)$$

where the unit of average concentration C_{AC} is ppm; $\int_0^t C dt$ is the integral of the gas concentration over the response time; τ is the burnout time, seconds.

(2) Calculation of NO_x volume (V_g)

Since the volumes of NO_x and CO are negligible compared to the input air, the volume of NO_x is approximately

$$V_g = Q \times \tau \times \frac{C_{AC}}{10^6} \quad (2)$$

where the unit of gas volume V_g is L; Q is the input airflow, L/s.

3. Results and Discussion

3.1. The Effect of Combustion Temperature on CO Emission from Fast-Growing Grass Combustion

Generally, volatile-N to volatile-NO_x and char-N to char-NO_x are the two main sources of NO_x in the flue gas. In the process of biomass utilization, the temperature of the boiler furnace is usually controlled below 900 °C, and the conversion of the fuel-N also occurs

at this temperature [39,40]. The subsequent measurements and analysis were conducted below 900 °C.

In the early stage, we studied the NO_x emission characteristics of fast-growing grass at 600, 700, 750, 800, and 850 °C. Please refer to the preliminary work for details [9]. From the results of our experiment, we observe that at 600 °C, the NO_x generated by volatile combustion is delayed (65 s). In addition, the concentration is low, about 20 ppm, and the combustion reaction lasts for nearly 180 s. Second, there are two peaks of NO_x emission during the combustion at 700, 750, 800, and 850 °C, corresponding to the volatile and semi-char combustion phase. Specifically, the first peak value is at about 20 s, and the peak value gradually increases with the increase in temperature. The second peak appears at 77, 58, 62, and 67 s, respectively, and the intensity is much lower than the first peak.

Following this, the flue gas measurements and analysis are also conducted on the CO emission generated by the burning of fast-growing grass under these five temperatures, and the results are shown in Figure 3.

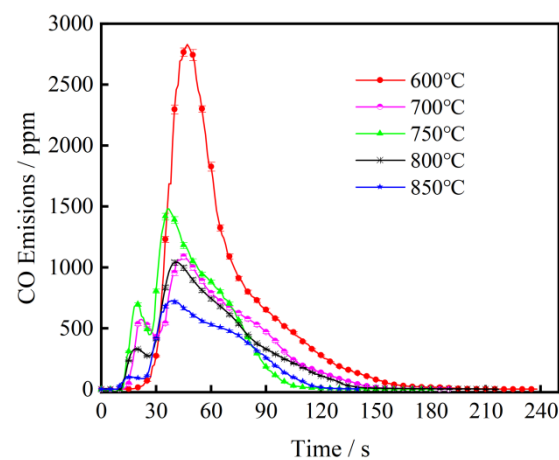


Figure 3. CO emission curve of fast-growing grass combustion at different temperature.

It is evident from Figure 3 that when the combustion temperature is 600 °C, the maximum peak value of the CO emission curve is attained (2830 ppm), which is 28.16 times that of the minimum peak value (100.5 ppm). In addition, when the temperature rises to 700, 750, 800, and 850 °C, respectively, the first peak appears quickly, around 20 s. With a subsequent increase in temperature, the peak values show a decreasing delineation of 573.5, 697.5, 333.0, and 100.5 ppm, respectively; in addition, the peak emission also narrows. The analysis shows that the behavior of the formation of CO is closely related to temperature. Different from 600 °C, a second peak appears at 700, 750, 800, and 850 °C in the CO emission curve at about 46, 38, 42, and 39 s, respectively. With the subsequent increase in temperature, the peak decreases in a similar way as the first peak, however, the peak is higher than the first peak. Specifically, the peaks are 1090.5, 1479.5, 1044.5, and 723 ppm, respectively, which is similar to the burning rule of large particle wood briquette fuel in Chen Guohua's research at 800 °C [41]. This may be because when the fast-growing grass fuel is just sent into the reactor the heat transfer rate between its interior and the surface is small; therefore, a small amount of CO-containing volatilization is released and gradually increases. When the surface temperature of the fast-growing grass fuel reaches the ignition point, the volatile content is ignited and begins to burn; subsequently, the CO concentration starts to drop, and, thus, the first peak appears. As the combustion continues, the heat continuously accumulates in the fast-growing grass fuel, accelerating the release of volatile matter, which causes the combustion reaction to intensify. At this time, the instantaneous consumption of O₂ on the fuel surface increases while the airflow is constant; thus, an anoxic atmosphere is formed, which generates a large amount of CO. When the volatilized output reaches the maximum value, the CO emission curve attains a second peak, and the volatilized output at this time is greater than the amount of volatilized output during

ignition; therefore, the second peak is higher than the first peak [41]. It is interesting to note that the peak CO emission of fast-growing grass burning at 750 °C is higher than that at 700 °C. This may be because 750 °C is the transition temperature from incomplete combustion to complete combustion. The research of Xu [42] shows a similar situation.

The total emissions of CO from fast-growing grass combustion at different temperatures are shown in Figure 4. It is evident from Figure 4 that the total CO emissions in the combustion process generally demonstrate a downward delineation with an increase in temperature. Specifically, when the temperature is 600 °C, the maximum value of CO emission is 1.899 mL, while when the temperature rises to 850 °C, the emission value is 0.619 mL, which is only 0.33 times the former. In addition, it is worth noting that in the range of 700–800 °C the temperature has little impact on the total emissions of CO; hence, the three emission curves are very close. When the temperature is 700 °C, the CO emission is 1.018 mL. When the temperature rises to 800 °C the CO emission only decreases to 0.912 mL, while at 750 °C, the CO emission exceeds the 700 °C emission. These results are consistent with the emission rule in Figure 3. Furthermore, considering that the emissions of CO (1.029 mL) and NO_x (0.025 mL) [9] are large at 750 °C, the subsequent experiments are conducted at this temperature.

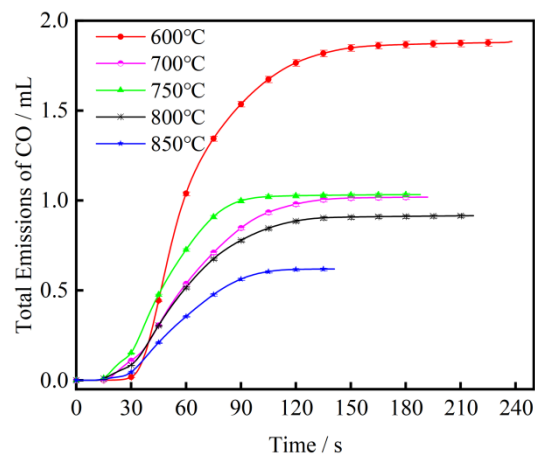


Figure 4. Total CO emission curve of fast-growing grass combustion at different temperatures.

3.2. The Effect of CaO on CO Emission

At 750 °C, the CO emission curves from the mixed combustion of fast-growing grass and CaO additives with different mass fractions (3, 5, 10, and 15%) are shown in Figure 5.

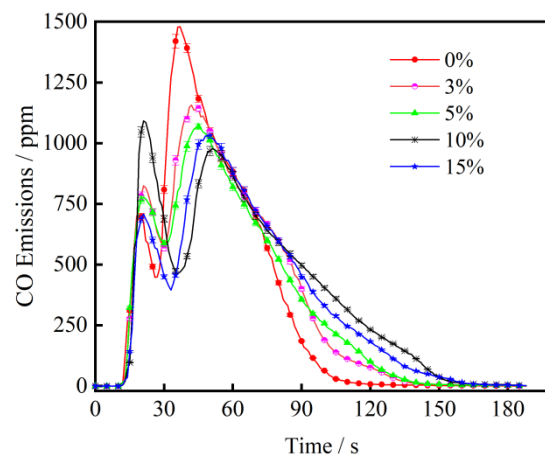


Figure 5. CO emission curve of fast-growing grass combustion with CaO additive at 750 °C.

As can be observed from Figure 5, introducing the CaO additive at 750 °C can reduce the maximum peak of the CO emission in the fast-growing grass combustion. This is because CaO additive can reduce CO emission in the early stage of combustion. At the same time, the effect of different mass fractions of CaO on CO emission varies. Except for the case of 10% additive, the maximum peak CO emission decreases with the increase of CaO additive. When the mass fraction of CaO is 3, 5, 10, and 15%, the maximum peak CO emission decreases by 21.83, 27.81, 26.24, and 30.34%, respectively, relative to the highest peak (1479.5 ppm) without additive. However, after 73 s, the presence of the CaO additive leads to an increase in the concentration of the CO emission and, much more, the extension of the combustion time. At the same time, after adding CaO additives, the first peak value increases to a certain extent, which may be due to the reaction of CaO with HCN in volatile matter of fast-growing grass to generate CO ($\text{CaO} + 2 \text{HCN} \rightarrow \text{CaCN}_2 + \text{CO} + \text{H}_2$) [35]. However, the increase of the peak value does not follow a clear rule with additives. When the mass fraction of CaO is 3, 5, 10, and 15%, the peak value increases by 127, 79.5, 393.8 and 11.2 ppm, respectively. Generally speaking, 10% CaO additive is a special value, similar to 750 °C in Section 3.1, which may be the inflection point value generated by CO. Zhang et al. [43] noticed a similar phenomenon when they studied the effect of CaO granulated blast furnace slag on denitration performance. The internal mechanism is worth further study. Therefore, to better analyze the CO emission from the mixed combustion of fast-growing grass and CaO additives with different mass fractions at 750 °C, the curve of the total CO emission over time is obtained. See Figure 6 for details.

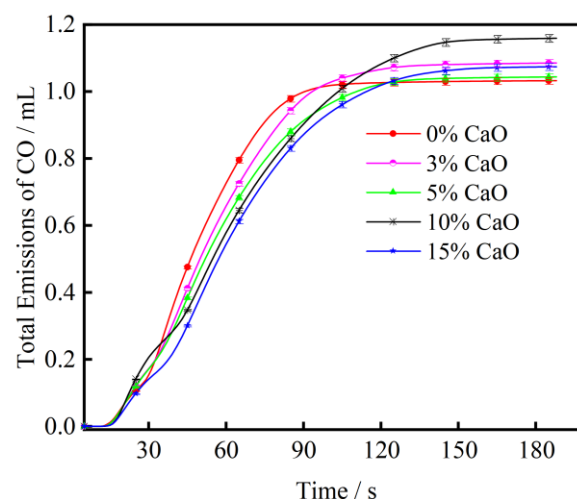


Figure 6. Total CO emission curve of fast-growing grass combustion with CaO additive at 750 °C.

It is obvious from Figure 6 that the total CO emission from fast-growing grass combustion rises after adding CaO additive compared with no additive. This is because, in the late combustion period, CaO and ash mix together covering the fuel surface; this reduces the contact area between the remaining unburned fuel and oxygen to some extent. As a consequence, beyond making the fast-growing grass produce a little CO during oxygen-poor combustion, it also prolongs the reaction time, thereby making the total CO emission increase slightly. Particularly, the CO emission curves are not linear with CaO mass fractions. When the 3, 5, and 15% CaO additives are added, respectively, the total CO emission is similar. However, when the 10% CaO additive is added the total CO emission is highest (1.17 mL), which is 13.59% more than the value obtained without the CaO additive (1.03 mL). Therefore, it is not recommended to add a 10% CaO additive.

3.3. The Effect of CaO on NO_x Emission

As shown in Figure 7, the CaO additive can inhibit the generation of volatile-NO_x and char-NO_x. Specifically, at 750 °C, after adding 3, 5, 10, and 15% CaO additives,

respectively, the first peak value of NO_x emission from fast-growing grass combustion decreased significantly by 42.55, 47.05, 39.01, and 40.89%, respectively. This is because CaO can catalyze HCN to generate N_2 , as shown in the equation $2 \text{C}_i\text{H}_j + 2 \text{HCN} \rightarrow \text{N}_2 + (j + 1 - k) \text{H}_2 + 2 \text{C}_{i+1}\text{H}_k$ [44]; in addition, CaO can also react with HCN and NH_3 in the pyrolysis stage to form N_2 , as shown in the equations $\text{CaO} + 2 \text{HCN} \rightarrow \text{CaCN}_2 + \text{CO} + \text{H}_2$; $\text{CaC}_x\text{N}_y \rightarrow \text{CaC}_x + y/2 \text{N}_2$; and $\text{CaC}_x + y \text{NH}_3 \rightarrow \text{CaC}_x\text{N}_y + 3/2 y \text{H}_2$ [33,45,46]. Surprisingly, adding more additives does not show a better peak reduction effect. This is due to the fact that the number of active sites decreases when the amount of additives reaches a particular level because the active ingredients agglomerate or cover the additives' surfaces. Similar findings have been noted in earlier research [16,47]. In addition, the second peak of the NO_x emission from fast-growing grass combustion also decreases, especially when the mass fraction of CaO is more than 3%, and the second peak almost disappears. This may be attributed to the delayed effect of CaO on CO release (see Figure 5). When char- NO_x is generated, CO still maintains a high concentration, which is not conducive to the formation of char- NO_x under the reduction environment. At the same time, it was also found that the CaO additive not only affects the peak emission of NO_x , but it also delays the occurrence of the two peaks.

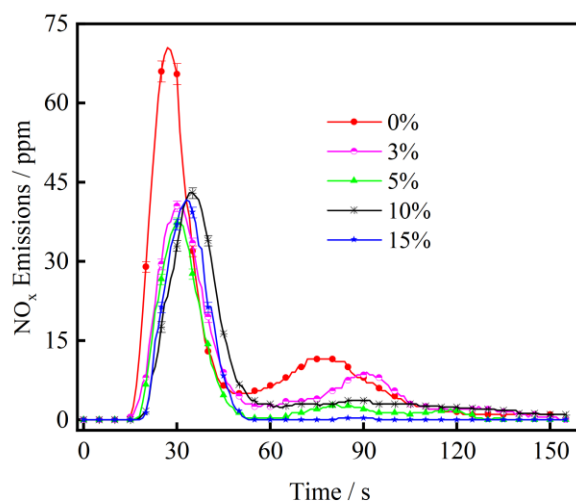


Figure 7. NO_x emission curve of fast-growing grass combustion with CaO additive at 750 °C.

It can be observed from Figure 8 that the CaO additive has a significant reduction effect on the total NO_x emission of fast-growing grass combustion which varies from the CaO mass fraction. It is worth noting that the emission reduction rate of NO_x is not directly related to the mass fraction of CaO. The emission reduction effect is worst at 10%, with a value of 26.13%. However, it is stronger when the mass fraction of CaO is 5% and 15%, and the values are 56.81% and 56.06%, respectively. This may be attributed to the mutual inhibition relationship between CO and NO_x . When the CaO mass fraction is 10%, the emission concentration of CO is the lowest in the 36–51 s period (also a crucial time for volatile- NO_x generation; see Figure 5); therefore, at this time, its ability to inhibit NO_x generation is at its lowest. As a result, the peak emission of NO_x generation occurs during this period (see Figure 7), which is the worst effect of the 10%. Considering the two factors of NO_x the peak and total emissions, it can be concluded that the 5% CaO additive achieves the best comprehensive control effect on NO_x emission from the combustion of fast-growing grass.

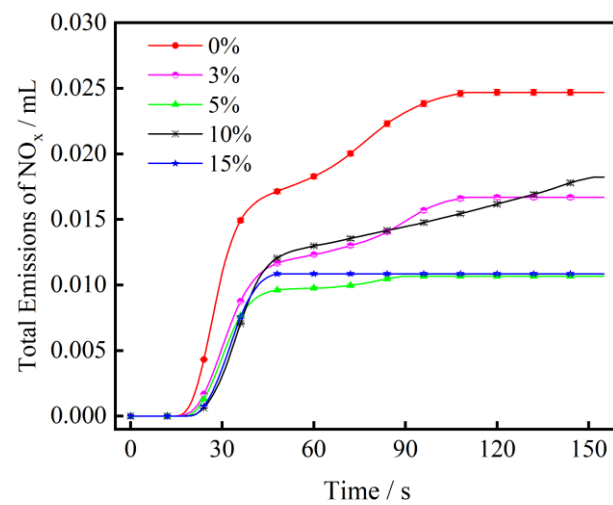


Figure 8. Total NO_x emission curve of fast-growing grass combustion with CaO additive at 750 °C.

4. Conclusions

In this paper, a self-built tubular furnace experimental platform was used to investigate the emission reduction characteristics of NO_x and CO from fast-growing grass combustion at different temperatures with different mass fractions of CaO additives. The following conclusions were drawn:

(1) Temperature is an important factor that affects CO emission from biomass combustion. With the increase in temperature, the CO emission curve attains a second peak higher than the first peak, and both the peak and total emissions show a decreasing trend (except 750 °C).

(2) CaO additive influences NO_x emission from fast-growing grass combustion. Specifically, at 750 °C, it reduces the peak and total emissions of NO_x. At the same time, considering the two factors, it is concluded that 5% CaO additive achieves the best comprehensive control effect on NO_x emission from fast-growing grass combustion, with the peak and total emissions reduction of 47.05% and 56.81%, respectively.

(3) CaO additive also has an important impact on CO emission from fast-growing grass combustion. CaO additive reduces the peak emission of CO to a certain extent but increases the total emission of CO.

In order to further expand the research findings of this paper, it is necessary to observe the surface morphology of fast-growing grass after adding CaO additive using a scanning electron microscope in order to further analyze the mechanism of CaO on CO and NO_x emissions.

Author Contributions: Data curation, Q.H. and Y.L.; investigation, Q.H. and Y.L.; methodology, H.L. (Heyun Liu); Project administration, H.L. (Haili Liu) and H.L. (Heyun Liu); writing-original draft, Y.L.; writing-review & editing, Y.L. and H.L. (Haili Liu). All authors have read and agreed to the published version of the manuscript.

Funding: This research was funded by the Hunan Provincial Natural Science Foundation of China (2021JJ50132) and the Youth Science and Technology Project of Hunan University of Humanities and Technology (2020QN05).

Data Availability Statement: All data used to support the findings of this study are included within the article.

Conflicts of Interest: The authors declare no conflict of interest.

Nomenclature

C	the concentration
V	the volume
M	the molar mass
Q	the input airflow
T	the temperature of the materials(K)
Abbreviations and acronyms	
AlNH ₄ (SO ₄) ₂	Ammonium Aluminum Sulfatehydrate
Ca	CalCium
CaCN ₂	CalCium Cyanamide
CaO	CalCium Oxide
CFB	CirCulating Fluidized Bed
Cl	Chlorine
CO	Carbon Monoxide
CO ₂	Carbon Dioxide
CuCl ₂	CupriC Chloride
Cu(NO ₃) ₂	CupriC Nitrate
H ₂	Hydrogen
HCN	Hydrogen Cyanide
H ₂ PtCl ₆	ChloroplatiniC ACid
K	Potassium
K ₂ CO ₃	Potassium Carbonate
KMnO ₄	Potassium Permanganate
MgO	Magnesium Oxide
MnO ₂	Manganese Dioxide
N ₂	Nitrogen
Na ₂ CO ₃	Sodium Carbonate
NH ₃	Ammonia
NH ₄ MgPO ₄	Magnesium Ammonium Phosphate
NO _x	Nitrogen Oxides, NO, N ₂ O
PM	PartiCulate Matter
S	Sulfur
SiC	SiliCon Carbide
TiO ₂	Titanium Dioxide
ZnCl ₂	ZinC Chloride

References

- Chen, C.; Fan, D.; Zhao, J.; Qi, Q.; Huang, X.; Zeng, T.; Bi, Y. Study on microwave-assisted co-pyrolysis and bio-oil of *Chlorella vulgaris* with high-density polyethylene under activated carbon. *Energy* **2022**, *247*, 123508. [[CrossRef](#)]
- Zhongming, Z.; Linong, L.; Xiaona, Y.; Wangqiang, Z.; Wei, L. *Global Energy Review 2021*; IEA: Paris, France, 2021.
- Wang, K.; Khoo, K.S.; Chew, K.W.; Selvarajoo, A.; Chen, W.; Chang, J.; Show, P.L. Microalgae: The future supply house of biohydrogen and biogas. *Front. Energy Res.* **2021**, *9*, 660399. [[CrossRef](#)]
- Recalde, M.; Woudstra, T.; Aravind, P.V. Gasifier, solid oxide fuel cell integrated systems for energy production from wet biomass. *Front. Energy Res.* **2019**, *7*, 129. [[CrossRef](#)]
- Mu, L.; Li, T.; Wang, Z.; Shang, Y.; Yin, H. Influence of water/acid washing pretreatment of aquatic biomass on ash transformation and slagging behavior during co-firing with bituminous coal. *Energy* **2021**, *234*, 121286. [[CrossRef](#)]
- Kobyłecki, R.; Zarzycki, R.; Bis, Z.; Panowski, M.; Wiński, M. Numerical analysis of the combustion of straw and wood in a stoker boiler with vibrating grate. *Energy* **2021**, *222*, 119948. [[CrossRef](#)]
- Lei, X. Carbon sink grass and its carbon sink mechanism. *Agric. Eng.* **2015**, *5*, 38–43.
- Lei, X. Comprehensively carry out general secretary Xi Jinping's important strategic thought on ecological civilization construction. *Energy China* **2017**, *668*, 101–107.
- Liu, H.; Hong, Q.; Liu, H.; Huang, Z.; Zhang, X.; Chen, W.; Zeng, X.; Pan, S. Effects of temperature and additives on NO_x emission from combustion of Fast-Growing grass. *Front. Energy Res.* **2021**, *9*, 772755. [[CrossRef](#)]
- Hu, B. Strength and Thermal Properties of Pennisetum—Gypsum Wall Material. Master's Thesis, Hunan University, Changsha, China, 2018.
- Nie, S.; Li, Q.; Li, P.; Wu, Q.; Liu, K. Pavement performance of fast-growing grass fiber asphalt mixture. *Highw. Eng.* **2021**, *46*, 183–187.

12. Wang, Q. The Preparation and Characterization of Fast-Growing Wood/Plastic Composites. Master's Thesis, Central South University of Forestry & Technology, Changsha, China, 2018.
13. Szatyłowicz, E.; Skoczko, I. Evaluation of the PAH content in soot from solid fuels combustion in low power boilers. *Energies* **2019**, *12*, 4254. [[CrossRef](#)]
14. Xu, Q.; Wang, S.; Jiang, J.; Bhattarai, N.; Li, X.; Chang, X.; Qiu, X.; Zheng, M.; Hua, Y.; Hao, J. Nitrate dominates the chemical composition of PM_{2.5} during haze event in Beijing, China. *Sci. Total Environ.* **2019**, *689*, 1293–1303. [[CrossRef](#)]
15. Liu, Y.; Gao, F.; Yi, H.; Yang, C.; Zhang, R.; Zhou, Y.; Tang, X. Recent advances in selective catalytic oxidation of nitric oxide (NO-SCO) in emissions with excess oxygen: A review on catalysts and mechanisms. *Environ. Sci. Pollut. Res.* **2021**, *28*, 2549–2571. [[CrossRef](#)] [[PubMed](#)]
16. Yu, Z.; Fan, X.; Gan, M.; Chen, X. Effect of Ca-Fe oxides additives on NO_x reduction in iron ore sintering. *J. Iron Steel Res. Int.* **2017**, *24*, 1184–1189. [[CrossRef](#)]
17. Zamansky, V.M.; Lissianski, V.V.; Maly, P.M.; Ho, L.; Rusli, D.; Gardiner, W.C., Jr. Reactions of sodium species in the promoted SNCR process. *Combust. Flame* **1999**, *117*, 821–831. [[CrossRef](#)]
18. Bae, S.W.; Roh, S.A.; Kim, S.D. NO removal by reducing agents and additives in the selective non-catalytic reduction (SNCR) process. *Chemosphere* **2006**, *65*, 170–175. [[CrossRef](#)] [[PubMed](#)]
19. Niu, S.; Han, K.; Lu, C. Experimental study on the effect of urea and additive injection for controlling nitrogen oxides emissions. *Environ. Eng. Sci.* **2010**, *27*, 47–53. [[CrossRef](#)]
20. Gasnot, L.; Dao, D.Q.; Pauwels, J.F. Experimental and kinetic study of the effect of additives on the ammonia based SNCR process in low temperature conditions. *Energy Fuels* **2012**, *26*, 2837–2849. [[CrossRef](#)]
21. Wang, F.; Chen, T.; Jin, M.; Lu, P. Simultaneous Desulfurization and Denitrification from Flue Gas Using Urea/Piperazine Solution. *Adv. Mater. Res.* **2014**, *881–883*, 641–644. [[CrossRef](#)]
22. Chen, C.; Chen, F.; Cheng, Z.; Chan, Q.; Kook, S.; Yeoh, G. Emissions characteristics of NO_x and SO₂ in the combustion of microalgae biomass using a tube furnace. *J. Energy Inst.* **2017**, *90*, 806–812. [[CrossRef](#)]
23. Liu, C.; Liu, J.; Evrendilek, F.; Xie, W.; Kuo, J.; Buyukada, M. Bioenergy and emission characterizations of catalytic combustion and pyrolysis of litchi peels via TG-FTIR-MS and Py-GC/MS. *Renew. Energy* **2020**, *148*, 1074–1093. [[CrossRef](#)]
24. Ulusoy, B.; Anicic, B.; Zhao, L.; Lin, W.; Lu, B.; Wang, W.; Dam-Johansen, K.; Wu, H. Multifunctional additives for NO_x abatement in fluidized bed biomass combustion. *Energy Fuels* **2021**, *35*, 12367–12379. [[CrossRef](#)]
25. Liu, X.; Yang, X.; Xie, G.; Yu, Y. NO emission characteristic during fluidized combustion of biomass with limestone addition. *Fuel* **2021**, *291*, 120264.
26. Gaze, B.; Knutel, B.; Jajczyk, M.; Waclawek, A.; Bukowski, P.; Dębowski, M. Analysis of the use of catalytic additives for combustion with wood pellets in a low-power boiler. *Rynek Energii* **2021**, *4*, 93–98.
27. Gaze, B.; Romanski, L.; Kulazynski, M. The concept of using urea to reduce NO (x) emissions from low power biomass boilers. *Przem. Chem.* **2020**, *99*, 569–573.
28. Gaze, B.; Hrywna, D.; Romanski, L.; Kulazynski, M. Effect of fuel type and active substance addition on exhaust gas emissions from vehicles powered by a spark ignition engine. *Przem. Chem.* **2021**, *100*, 73–78.
29. Meng, J.; Zhang, X.; Ai, Y.; Yue, H.; Li, X.; Chen, R. Deslagging of Eichhornia crassipes and Pistia stratiotes biomass pellets. *Energy Rep.* **2021**, *7*, 822–829. [[CrossRef](#)]
30. Lindström, E.; Sandström, M.; Boström, D.; Öhman, M. Slagging characteristics during combustion of cereal grains rich in phosphorus. *Energy Fuels* **2007**, *21*, 710–717. [[CrossRef](#)]
31. Najser, T.; Gaze, B.; Knutel, B.; Verner, A.; Najser, J.; Mikeska, M.; Chojnacki, J.; Němček, O. Analysis of the effect of catalytic additives in the agricultural waste combustion process. *Materials* **2022**, *15*, 3526. [[CrossRef](#)]
32. Zhang, H.; Gong, Z.; Liu, L.; Wang, Z.; Li, X. Study on the migration characteristics of sulfur and nitrogen during combustion of oil sludge with CaO additive. *Energy Fuels* **2020**, *34*, 6124–6135. [[CrossRef](#)]
33. Liu, H.; Zhang, Q.; Hu, H.; Liu, P.; Hu, X.; Li, A.; Yao, H. Catalytic role of conditioner CaO in nitrogen transformation during sewage sludge pyrolysis. *Proc. Combust. Inst.* **2015**, *35*, 2759–2766. [[CrossRef](#)]
34. Xing, X.; Xing, Y.; Yu, J.; Li, Y.; Ma, P.; Xu, B. Characteristics of CO and NO emission from municipal solid waste combustion. *Chin. J. Process Eng.* **2017**, *17*, 866–872.
35. Hayhurst, A.N.; Lawrence, A.D. The effect of solid CaO on the production of NO_x and N₂O in fluidized bed combustors: Studies using pyridine as a prototypical nitrogenous fuel. *Combust. Flame* **1996**, *105*, 511–527. [[CrossRef](#)]
36. Leckner, B.; Karlsson, M.; Mjornell, M.; Hagman, U. Emissions from a 165 MWth circulating fluidised-bed boiler. *J. Inst. Energy* **1992**, *65*, 122–130.
37. Liu, X.; Luo, Z.; Yu, C. Effect of limestone on the emission of NO during petroleum coke combustion. *Fuel* **2018**, *224*, 1–9. [[CrossRef](#)]
38. Xu, G.; Ou, J.; Fang, B.; Wei, H.; Hu, T.; Wang, H. NO_x emission from the combustion of mixed fuel pellets of Fenton/CaO-conditioned municipal sludge and rice husk. *Environ. Pollut.* **2021**, *281*, 117018. [[CrossRef](#)]
39. Vermeulen, I.; Block, C.; Vandecasteele, C. Estimation of fuel-nitrogen oxide emissions from the element composition of the solid or waste fuel. *Fuel* **2012**, *94*, 75–80. [[CrossRef](#)]
40. Shah, I.A.; Gou, X.; Wu, J. Simulation study of an Oxy-Biomass-Based boiler for nearly zero emission using aspen plus. *Energies* **2019**, *12*, 1949. [[CrossRef](#)]

41. Chen, G.; Li, Y.; Peng, H.; Li, Y.; Jiang, Z. Characteristics of flue gas emissions during large wood pellet combustion. *Trans. Chin. Soc. Agric. Eng.* **2015**, *31*, 215–220.
42. Xu, Q.; Peng, W.; Ling, C. An experimental analysis of soybean straw combustion on both CO and NO_x emission characteristics in a tubular furnace. *Energies* **2020**, *13*, 1587. [[CrossRef](#)]
43. Zhang, L.; Jia, Y.; Shu, H.; Zhang, L.; Lu, X.; Bai, F.; Zhao, Q.; Tian, D. The effect of basicity of modified ground granulated blast furnace slag on its denitration performance. *J. Clean. Prod.* **2021**, *305*, 126800. [[CrossRef](#)]
44. Tan, H.; Wang, X.; Wang, C.; Xu, T. Characteristics of HCN removal using CaO at high temperatures. *Energy Fuels* **2009**, *23*, 1545–1550. [[CrossRef](#)]
45. Fu, S.; Song, Q.; Tang, J.; Yao, Q. Effect of CaO on the selective non-catalytic reduction deNO_x process: Experimental and kinetic study. *Chem. Eng. J.* **2014**, *249*, 252–259. [[CrossRef](#)]
46. Zhang, Q.; Liu, H.; Lu, G.; Yi, L.; Hu, H.; Chi, H.; Yao, H. Mechanism of conditioner CaO on NO_x precursors evolution during sludge steam gasification. *P. Combust. Inst.* **2017**, *36*, 4003–4010. [[CrossRef](#)]
47. Sun, J.; Zhao, B.; Su, Y. Advanced control of NO emission from algal biomass combustion using loaded iron-based additives. *Energy* **2019**, *185*, 229–238. [[CrossRef](#)]

Disclaimer/Publisher’s Note: The statements, opinions and data contained in all publications are solely those of the individual author(s) and contributor(s) and not of MDPI and/or the editor(s). MDPI and/or the editor(s) disclaim responsibility for any injury to people or property resulting from any ideas, methods, instructions or products referred to in the content.